Journal of Materials Chemistry B

ROYAL SOCIETY OF CHEMISTRY

PAPER

View Article Online
View Journal | View Issue

Cite this: J. Mater. Chem. B, 2025, 13, 4657

Modulation of the biological response to surfaces through the controlled deposition of 3D polymeric surfactants†

Valentina Cuzzucoli Crucitti,*[ab] Hadi Hajiali, ‡[c] Adam A. Dundas,[b] Vineetha Jayawarna,[d] Dario Tomolillo,[e] Iolanda Francolini,[f] Claudia Vuotto,[e] Manuel Salmeron-Sanchez,[d] Matthew J. Dalby,[g] Morgan R. Alexander,[c] Ricky D. Wildman,[ab] Felicity R. A. J. Rose *[c] and Derek J. Irvine *[ab]

Received 28th August 2024,
Accepted 5th March 2025

DOI: 10.1039/d4tb01941e

rsc.li/materials-b

Biomaterials play a crucial role in modern medicine through their use as medical implants and devices. However, they can support biofilm formation and infection, and lack integration with the surrounding human tissue at the implant site. This work reports the development of novel poly(ethyl acrylate) (PEA) based copolymers that address both issues. These PEA materials were molecularly designed polymeric surfactants (surfmers) synthesised *via* controlled radical polymerisations to achieve different polymeric architectures, (*i.e.*, statistical and block copolymers). These were both deposited as structured 2D films on glass coverslips and used to manufacture monodisperse 3D micro-particles with functional surfaces (*via* microfluidics). ToF-SIMS was used to analyse these 2D and 3D surfaces to understand: (a) the surface arrangement of the monomer sequences exhibited by the different polymer structures and (b) how this surface monomer arrangement influenced mammalian fibroblast cell and/or *Staphylococcus aureus* behaviour at these film/particle surfaces. In addition, the form of the fibronectin (FN) network assembly's importance in promoting growth factor (GF) binding was probed using atomic force microscopy (AFM) on the 2D films. This confirmed that specific surfmer molecular surface organisations were achieved during film/micro-particle fabrication, which presented exterior functionalities that either prevent biofilm attachment or promote the formation of structured FN networks for GF binding.

Introduction

There is a significant body of research focussed on the control of both bacterial and mammalian cell behaviour on materials surfaces to address issues associated with infections related with medical devices[1] and as part of regenerative medicine strategies to modulate mammalian cell behaviour and promote tissue repair.[2–4]

Bacterial biofilm formation has been identified as a principal route to device associated infection,[5–7] and increased tolerance to antibiotic treatment when compared to planktonic counterparts.[8,9] Biomaterial strategies have been developed to prevent the irreversible attachment of biofilms or to kill the surface contacting microbes by the inclusion of biocidal additives, such as silver ions.[10–12] Furthermore, this material performance has also been successfully transferred from two dimensional (2D) to three dimensional (3D) device surfaces (*i.e.*, from flat films to surface coatings of 3D structures such as tubes and particles).[13,14] These 3D coatings were achieved by synthesising amphiphilic copolymers that included hydrophobic, high-throughput (HT) identified, biofilm resistant monomers.

[a] Centre for Additive Manufacturing, Faculty of Engineering, University of Nottingham, Nottingham NG7 2RD, UK. E-mail: Valentina.CuzzucoliCrucitti1@nottingham.ac.uk, Derek.Irvine@nottingham.ac.uk
[b] Department of Chemical and Environmental Engineering, Faculty of Engineering, University of Nottingham, Nottingham NG7 2RD, UK
[c] School of Pharmacy, Nottingham Biodiscovery Institute, Faculty of Science, University of Nottingham, Nottingham NG7 2RD, UK. E-mail: Felicity.Rose@nottingham.ac.uk
[d] Centre for the Cellular Microenvironment, School of Engineering, Advanced Research Centre, University of Glasgow, Glasgow G11 6EW, UK
[e] Neuromicrobiology Unit, IRCCS Fondazione Santa Lucia, Rome, Italy
[f] Dept of Chemistry, Sapienza University of Rome, Piazzale A. Moro 5, 00185 Rome, Italy
[g] Centre for the Cellular Microenvironment, School of Molecular Biosciences, College of Medical, Veterinary and Life Sciences, Advanced Research Centre, University of Glasgow, Glasgow G11 6EW, UK

† Electronic supplementary information (ESI) available. See DOI: https://doi.org/10.1039/d4tb01941e

‡ Current address: Healthcare Technologies Institute, Institute of Translational Medicine, School of Chemical Engineering, University of Birmingham, Birmingham, B15 2TT, UK.

Such copolymer coatings have been demonstrated to avoid bacterial attachment on a commercial urinary catheter.[15]

Materials research has also focussed on the ability to support tissue regeneration, manipulating the biomaterial surface based on the targeted site which is essential for achieving optimal biological performance.[16] As an example, Ranella *et al.* explored how fibroblast cells adhere and survive on 3D silicon surfaces with varying roughness and wettability. They used femtosecond laser structuring to create surfaces with controlled micro- and nano-scale features and then adjusted surface chemistry without affecting the topography.[17] In addition, using different functional groups on the surface of biomaterials can stimulate different biochemical signalling pathways.[18–20] Zhang *et al.* investigated the potential proinflammatory influence of surface functional groups on human pulmonary epithelial cells and macrophages by using quantum dots coated with polymers containing various functional groups (–COOH, $–NH_2$, –OH, $–OCH_3$).[18] HT-screening platforms have played a key role in the study of manipulating biomaterial properties to influence stromal cell behaviour.[21,22] High-throughput screening experiments identified candidates that drive fibroblasts towards either pro- or antiproliferative functional phenotypes. In this study, poly(tetrahydro furfuryl acrylates) (pTHFuA) was used to support healing in chronic wounds when in particulate form.[23] These polymers were used to create bio-instructive surfactant materials termed 'surfmers' and then used to produce particles that significantly accelerated wound healing in animal models.

Microparticles, with bio-instructive surfaces that can be easily tailored by simply changing the identity of the surfmer, are of significant interest for cell-based therapies, as they provide a very high surface area for achieving intimate contact with the anatomical treatment area and require minimally invasive surgical procedures. Bone, in the form of bone graft, is the second most transplanted tissue after blood, with bone grafts used to replace tissue that is lost through damage or disease.[24] The healing process of a bone is also a multifaceted process that requires mechanical stability and revascularisation along with osteogenesis, osteoinduction and osteoconduction.[25] Consequently, several different materials strategies have been developed in recent years to achieve the goal of osteogenic repair, including the use of: (a) allogenic and autologous bone,[26–29] (b) decellularized bone matrix,[28] and (c) synthetic ceramic.[24,30] However, these materials do not actively promote bone healing or face challenges with regards to their supply and use clinically.

One promising route forward in bone repair is the localised delivery of physiologically relevant GF, including bone morphogenetic proteins (BMPs), directly to the implant site to locally regulate mesenchymal stromal cell (MSCs) behaviour and minimise off-target effects associated with supra-physiological doses when administered by injection. They promote differentiation of MSCs to osteoblasts responsible for the deposition of new bone and play a role in the repair of fractures.[31,32] The chemistry adopted in these studies included the use of poly(ethyl acrylate) (PEA) coatings, which we have previously shown to trigger the spontaneous assembly of FN molecules into biological networks.[33] The key advantage of this strategy resided in the fact that structured FN exposed specific domains shown to be highly effective for GF binding.[34] Interaction with these domains promoted simultaneous exposure of the integrin binding (FNIII9–10) and the GF binding (FNIII12–14) regions and so promoted binding and co-localisation of integrins and GF receptors.

An additional complication of bone regeneration, especially after a trauma or surgery, is osteomyelitis; an infection resulting from the formation of a persistent biofilm upon the tissue/implant of the host. As such, if osteomyelitis manifests itself during treatment, it can lead to complicated clinical scenarios often necessitating repeated surgical interventions to clear the infection.[35] Thus, the prevention of biofilm formation is a key goal in successfully achieving high quality and long-lasting bone fixation.

In this work, PEA candidate materials were synthesised in the form of surfmers for use in both the generation of structured 2D films and for the stabilisation of oil-in-water emulsions within a droplet-based microfluidics process to produce highly monodisperse 3D MPs in flow. To date, our research has focused on the performance of homo-polymers, statistical copolymers, or blends of homo-polymers in various applications, investigating the behaviour of biological systems on both 2D and 3D surfaces.[36] This study represents the first report of block copolymers being utilized in these applications, warranting an investigation into both their 2D and 3D performance. By including the results related to the MPs, we provide a comprehensive evaluation of the block copolymers' potential for innovative biomedical applications. This strategy was driven by the possibility of enabling the derivation of active PEA coatings to provide both non-bacterial killing anti-biofilm-attachment properties and allow the formation of a structured FN network to promote GF binding. Therefore, surface analysis was conducted to study how the surface chemistry and copolymer molecular structure, when applied to both a 2D (glass coverslip substrate) and 3D (MPs), affected mammalian cytotoxicity and adhesion (3T3 fibroblasts), fibronectin network assembly (GF binding promotion), and *S. aureus* attachment.

Materials and methods

Materials

All the materials were used as received unless stated otherwise. 2-(Dimethylamino)ethyl methacrylate (DMAEMA) (98%), ethyl acrylate (EA) (99%), 2,2′-azobis (2-methylpropionitrile) (AIBN, 98%) and the benzyl mercaptan (BzSH, 99%) were purchased from Sigma Aldrich. The cyclohexanone, acetone and heptane used as solvents for the synthesis and precipitation steps, respectively, were used as received and supplied by Fisher Scientific. In the ATRP, copper(I)bromide (98%) was purchased from Strem Chemicals UK LTD. Copper(I)chloride (99.99%) and copper(II)chloride (97%) were procured from Puratrem and Sigma-Aldrich, respectively. 1,1,4,7,10,10-Hexamethyltriethylenetetramine (HMTETA) (97%), ethyl α-bromoisobutyrate (EBriBru) (99%), *N*,*N*,*N*′,*N*″,*N*″-pentamethyldiethylenetriamine

(PMDETA) (99%) were obtained from VWR International LTD. Aluminium oxide (Al_2O_3) was obtained from Fisher Scientific. Murine 3T3 fibroblast cells (passage number 50–60) were obtained from the European Collection of Cell Cultures (ECACC, UK) and cultured in 75 cm^2 flasks (Nunc™, Fisher Scientific, Loughborough, UK) in Dulbecco's modified Eagle's medium (DMEM; Invitrogen, Paisley, UK) supplemented with 10% (v/v) foetal calf serum (FCS; Sigma-Aldrich Company Ltd, Dorset, UK), 2 mM L-glutamine solution (Sigma-Aldrich Company Ltd, Dorset, UK) and 1% (v/v) antibiotic/antimycotic solution (10 000 units per mL penicillin G, 100 mg mL^{-1} streptomycin sulphate and 25 μg mL^{-1} amphotericin B; Sigma-Aldrich Company Ltd, Dorset, UK).

Synthetic procedures

Thiol-mediated free radical polymerisation of homopolymers and statistical copolymers. The general procedure adopted for the thiol-controlled polymerisations to synthesise both the homopolymers poly(ethyl acrylate) (polyEA), poly(2-dimethylaminoethyl methacrylate) (polyDMAEMA) and the statistical poly(EA-*co*-DMAEMA) copolymers used as coatings in this study is both detailed below and shown in Scheme 1.

The appropriate quantities of the monomers were introduced into the required volume of cyclohexanone with stirring, such that a 1 : 3 v/v ratio mixture was achieved. In the case of the copolymers, these quantities also required to reach the targeted molar ratios, 90 : 10% mol/mol (*e.g.*, EA : DMAEMA 1.71 g : 0.29 g). The thiol CTA, benzyl mercaptan (BzSH) was added at the concentration of 1 mol% with respect to the monomers. The initiator, AIBN (0.5% wt with respect to the monomers) was, first, dissolved in cyclohexanone and degassed separately prior to being added to the reaction mixture. Finally, the reaction vessel and the AIBN solution were cooled in ice and then degassed by being purged with argon using a standard Schlenk line for at least 1 h. To commence the reaction, the temperature was raised to 75 °C in an oil bath and the reaction held at this temperature with continual stirring for 18 h. After this, the reaction vessel was cooled to room temperature to cease the reaction and then polymer purification was conducted *via* precipitation of the cooled reaction mixture into an excess of heptane. The typical non-solvent : reaction media ratio was 5 : 1 v/v to enhance the precipitation process and, finally, the precipitated materials were collected in a vial and left in a vacuum oven at 25 °C for at least 24 h.

^{1}H-NMR spectroscopic analysis was performed on the crude polymerisation solution to determine polymer conversion and, finally, on the precipitate to establish the actual monomer ratio of the final copolymer composition and to determine that the sample was free of any residual monomer. To evaluate the molar mass of the materials, the purified samples were dissolved in HPLC grade THF for GPC analysis. All the spectra data presented were collected at 400 MHz in $CDCl_3$ and values are quoted as δH ppm.

^{1}H-NMR of EA-*co*-DMAEMA purified (400 MHz, $CDCl_3$) δ (ppm): 4.12 (4H, C═OOCH_2, m), 2.55 (2H CH_2CH_2N, s), 2.28 (6H, NCH_3CH_3, s), 1.26 (3H, OCH_2CH_3, m).

^{13}C-NMR of EA-*co*-DMAEMA purified (400 MHz, $CDCl_3$) δ (ppm): 174 (C═O), 63.09, (C═OCH_2CH$_2$ DMAEMA), 60.25 (C═OCH_2CH$_3$), 56.77 (C═OCH$_2$CH_2 DMAEMA), 45.80 (NCH_3CH_3), 14.077 (OCH_2CH_3).

Synthesis of block EA-*b*-DMAEMA copolymers *via* atom transfer radical polymerisation

Synthesis of block 1 polyEA *i.e.*, the EA macroinitiator. The procedure for the synthesis of polyEA first block followed a

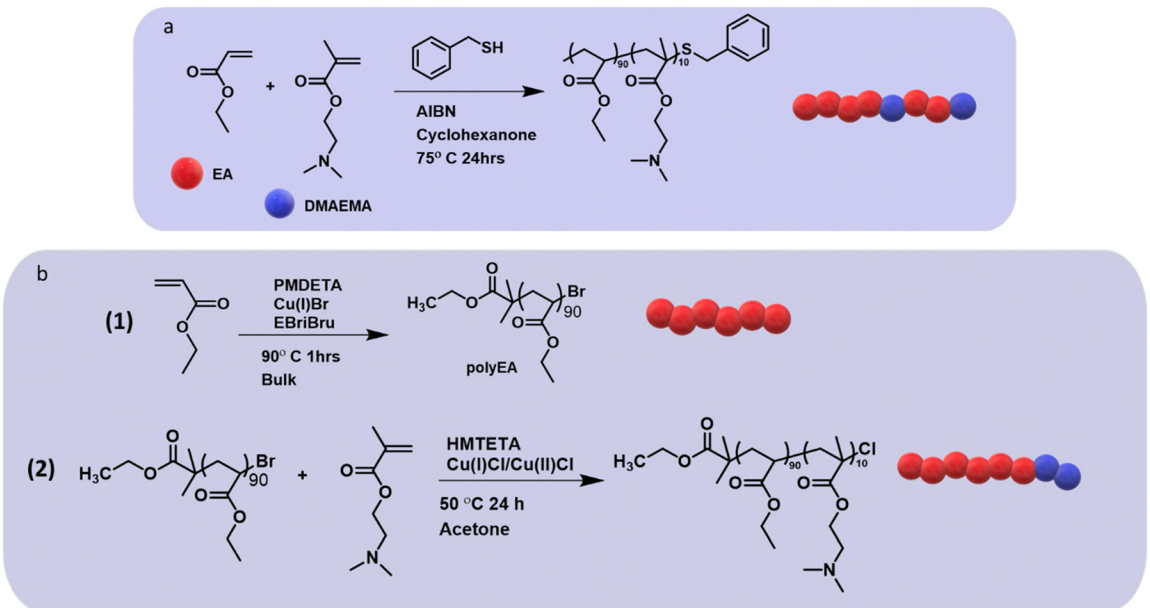

Scheme 1 Reaction schemes for the copolymerisations of ethyl acrylate (EA) (red sphere) and 2-(dimethylamino)ethyl methacrylate (DMAEMA) (blue sphere). (a) TFRP of EA-*co*-DMAEMA producing a random copolymer consisting in random (b) ATRP for EA-*b*-DMAEMA producing a block copolymer, involving the first step with the synthesis of polyEA (1) and second step with the growing of the second block of DMAEMA (2).

methodology literature reported method (Scheme 1).[37] Ethyl acrylate (EA) (2.5 g, 25 mmol) was added to a flask, followed by the required quantities of both α-bromoisobutyrate (EBriBru) (37 μL, 0.25 mmol) and *N*,*N*,*N*′,*N*″,*N*″-pentamethyldiethylenetriamine (PMDETA) (52.3 μL, 0.25 mmol) which was sufficient to deliver relative EA : EBriBru : Cu^{I} : PMDETA ratios of 130 : 1 : 1 : 1. After three freeze–pump thaw cycles, the mixture was added to Cu(I)Br (0.25 mmol, 35 mg) under argon atmosphere *via* canula. The reaction vessel was then purged with argon for 30 min, while stirring in the oil bath with the temperature set at 90 °C. After the reaction was conducted for a further 1 h at 90 °C, it was terminated by opening the flask to air and cooling to room temperature. The reaction mixture was then diluted with 10 mL dicholoromethane (DCM) and passed through a small neutral alumina column to remove the catalyst. The final pure product was obtained after precipitation into an excess of heptane as described in the statistical copolymer method section.

^{1}H-NMR spectroscopic analysis was performed on the crude polymerisation solution to determine polymer conversion and, finally, on the precipitate to establish the actual monomer ratio of the final copolymer composition and to determine that the sample was free of any residual monomer. To evaluate the molar mass and dispersity of the materials, the purified samples were dissolved in HPLC grade THF for GPC analysis. ^{1}H-NMR (400 MHz, $CDCl_3$) δ (ppm) = 1.23 (m, CH_2CH_3); 4.14 (m, OCH_2CH_3).

Synthesis of full EA-*b*-DMAEMA block copolymer. The general procedure adopted for the polymerisations, as shown in Scheme 1, was as follows based on a reported literature preparation.[38] The EA macroinitiator (0.031 mmol, 500 mg) and DMAEMA (1.1 mmol, 186 μL) was dissolved in acetone in a v/v ratio of 1 : 2.1 (monomers : acetone). Subsequently, Cu(I)Cl (0.063 mmol, 6.23 mg) and Cu(II)Cl (0.014 mmol, 1.7 mg) were added in the Schlenk flask. Finally, the ligand 1,1,4,7,10,10-hexamethyltriethylenetetramine (HMTETA) (0.062 mmol, 11.42 μL) was introduced immediately before starting the three freeze–pump thaw cycles, to minimise the interaction with the inorganic catalyst during the three cycles. The reaction was conducted for 24 h at a temperature of 50 °C with continuous stirring. The polymerisation was terminated by opening the flask to air and cooling to room temperature. The reaction mixture was then diluted with 10 mL THF and passed through a small neutral alumina column to remove the catalyst. The final pure product was obtained after precipitation into an excess of hexane.

^{1}H-NMR spectroscopic analysis was performed on the crude polymerisation solution to determine polymer conversion and, finally, on the precipitate to establish the actual monomer ratio of the final copolymer composition. To evaluate the molar mass and dispersity of the materials, the purified samples were dissolved in HPLC grade THF for GPC analysis.

^{1}H-NMR (400 MHz, $CDCl_3$) δ (ppm) = 1.23 (m, CH_2CH_3), 2.28 (s, NCH_3CH_3) 2.56 (m, CH_2CH_2N); 4.14 (m, OCH_2CH_3).

^{13}C-NMR (400 MHz, $CDCl_3$) δ (ppm) = 174 (C═O), 63.09, (C═OCH_2CH_2 DMAEMA), 60.25 (C═OCH_2CH_3), 56.77 (C═OCH_2-CH_2 DMAEMA), 45.80 (NCH_3CH_3), 14.077 (OCH_2CH_3).

Nuclear magnetic resonance spectroscopy (NMR). NMR spectra were recorded at 25 °C using Bruker AV400 and AV3400 spectrometers (400 MHz) and deuterated solvents. Chemical shifts were assigned in parts per million (ppm). ^{1}H-NMR and ^{13}C-NMR chemical shifts (δH, δC) are reported with the shift of $CDCl_3$ (δH = 7.26 ppm and δC = 77.0 ppm, respectively). Samples were dissolved in deuterated chloroform ($CDCl_3$) to which chemical shifts are referenced (residual chloroform at 7.26 ppm). MestReNova 14.2.1 copyright 2021 (Mestrelab Research S. L.) was used for analysing the spectra.

Gel permeation chromatography (GPC). GPC analysis was performed using an Agilent 1260 Infinity instrument equipped with a double detector with the light scattering configuration. Two mixed C columns at 35 °C were employed, using THF as the mobile phase with a flow rate of 1 mL min^{-1}. GPC samples were prepared in HPLC grade THF and filtered prior to injection. Analysis was carried out using Astra software. The number average molar mass (M_n) and dispersity ($Đ$) were calculated using PMMA for the calibration curve.

Dip-coating methodology. Dip-coating of glass cover slips (*d*: 130.00 mm, *t*: 0.16–0.19 mm) was achieved using a solution of 30 mg mL^{-1} of each synthesised polymer in DCM. Non treated glass cover slips were dip-coated twice and left to dry at room temperature for 24 h followed by 7 days in a vacuum oven at 25 °C.

Microparticle production method

Apparatus specification. Polymer microparticles were produced using a 100 μm hydrophilic 3D flow-focusing microfluidic droplet generator (Dolomite). Two syringe pumps (Havard Instrument) were used to deliver the continuous and dispersed flows to the microfluidic generator. The continuous phase used was DI water while, the dispersed phase contained the monomer (1,6 hexanediol diacrylate, 96% (w/v), Sigma-Aldrich) with 2% (w/v) polymeric surfactant and 2% (w/v) photoinitiator (2,2 dimethoxy-2-phenylacetophenone, Sigma-Aldrich).

Microfluidic methods. Once stable generation of the droplets was observed, the droplets were collected in a vial filled with 10 mL of DI water and placed inside a UV protective box. The capillary tube was then placed into the sample vessel, with the tip just slightly submerged in the water. The 365 nm UV fibre optic cable was aligned to the particle collection stream leaving the capillary tube. The production was continued for up to two hours or until enough sample was collected for post curing. After the polymeric droplets had undergone cross-linking, the UV was switched off and the polymer beads were filtered through a 40 μm nylon mesh filter. Microparticles were stored in the fridge (2–8 °C) until use.

Microparticle characterisation

Microparticle size and topography analysis. Dry samples were characterised using scanning electron microscopy (SEM). SEM imaging was performed using a JEOL JSM-6060LV, the dried microfluidic produced particles were sprinkled, using a spatula, onto double-sided adhesive carbon tape. Prior to SEM analysis, the samples were sputter-coated for 4–5 minutes at

25 mA with a thin gold layer in an argon atmosphere utilising a Leica EM SCD005 sputter coater (Leica Microsystems GmbH, Wetzlar, Germany) to give approximately a 25 nm thick coating. The diameters of the MPs were also determined using SEM using images captured at a magnification of 130×. Three separate images were taken from each sample (same batch), with 100 MP diameters being measured in each image using the Hough Circle Transform plugin within ImageJ (Fiji software).

Microparticle surface characterisation. Microparticles were placed onto a poly(hydroxyethyl) methacrylate substrate and subjected to mass-spectrometry using a ToF-SIMS IV instrument using a 25 keV Bi_3^+ primary ion source. Analysis for positive and negative spectra was acquired over a 500 μm × 500 μm scan area. Other analyses parameters were a cycle time of 100 μs, one shot/frame/pixel and 20 scans per analysis. As samples were non-conductive a 20 eV electron flood gun was applied. Image and spectra were acquired using SurfaceLab 6 software and analysed using SurfaceLab 7.1 software.

Mammalian cytocompatibility testing

Fibroblast cell culture. Murine 3T3 fibroblast cells were cultured in 75 cm^2 flasks with complete 3T3 media (Dulbecco's modified Eagle's medium (DMEM)), 10% (v/v) foetal calf serum, 2 mM L-glutamine solution, and 1% (v/v) antibiotic/antimycotic solution (10 000 units per mL penicillin G, 100 mg mL^{-1} streptomycin sulphate and 25 μg mL^{-1} amphotericin B). The medium was changed twice a week, with all cultures maintained in a humidified environment at 37 °C, 5% CO_2 in air.

Biological assessment of surfactant coated 2D surfaces. Dip-coated glass coverslips were placed into the wells of a non-tissue culture treated 24 well sterile plate (three replicates for each polymer sample). Coverslips were sterilised using UV exposure (254 nm) overnight and then further washed at room temperature prior to the addition of 400 μL fibronectin (20 μg mL^{-1} in DPBS; from R&D systems 1918-FN-02M) with incubation at 37 °C for one hour. Prior to seeding the 3T3 fibroblasts, the fibronectin solution was removed from the samples and the coverslips washed once with DPBS. Cells were seeded at a concentration of 50 000 cells per well in complete 3T3 media (supplemented with 10% (v/v) FCS) and incubated overnight at 37 °C in a controlled, humidified atmosphere (5% CO_2 in air). Samples were then investigated for cell adhesion, morphology and viability using Live/Dead™ staining and the Presto Blue assay (as described below).

Cell (3T3 fibroblast) adhesion and viability of cells using the Live/Dead™ assay. Assessment of mammalian (3T3 fibroblast) adhesion and viability was carried out using the Live/Dead™ Viability/Cytotoxicity Kit (ThermoFisher Scientific, UK) according to the manufacturer's instructions. Calcein AM and ethidium homodimer-1 were prepared in PBS to produce the Live/Dead™ staining solution and the solution transferred to the cells, for 30 minutes, replacing the overnight culture media. Live cells stained green (Calcein AM) and the nuclei of dead cells stained red (ethidium homodimer-1). Samples were washed in PBS and cells visualised using a Leica DR IRBE microscope, equipped with an automated stage and an attached Leica DC200 digital camera (Leica Microsystems Ltd, UK).

Cell (3T3 fibroblast) viability determined using the Presto Blue assay. PrestoBlue™ (Invitrogen, UK) was used as an assessment of 3T3 metabolic activity of cells adherent to the various coatings on coverslips (samples were assessed in triplicate; $n = 3$) according to the manufacturer's protocol. Briefly, 3T3 culture medium was replaced by PrestoBlue™: 3T3 culture medium (1 : 9) diluted in sterile PBS and incubated in the dark for 1.5 hours at 37 °C. Aliquots (100 μL) aliquots of the reagent were assessed for fluorescence at $\lambda_{exc}/\lambda_{em}$ 560/590 nm using a Tecan Infinite M200 microplate reader (Tecan, UK), and metabolic activity expressed as a percentage of the control (glass coverslip) as a measure of cell viability.

Assessment of fibronectin assembly on the surfactant coated coverslips. Atomic force microscopy (AFM) was used in air for imaging and characterising the surface topography of all conditions before and after FN adsorption. FN was adsorbed on different surfactant coated coverslips from solutions of 20 μg mL^{-1} in DPBS for 30 min, then washed with distilled water and dried with a nitrogen flow before analysis. A JPK Nanowizard 4 (JPK Instruments) system was used in tapping mode for imaging using antimony-doped Si cantilevers with a nominal resonant frequency of 75 kHz (RFESPA-75, Bruker). Height and phase images were acquired from each scan. The JPK Data Processing software versions 6 were used for image analysis.

Antibiofilm activities (EA-*b*-DMAEMA and EA-*co*-DMAEMA). The antibiofilm activity of the EA-*co*-DMAEMA and EA-*b*-DMAEMA against biofilm-forming *Staphylococcus aureus* CH 10850 MRSA cells were evaluated both by counting the number of CFUs per polymer surface unit (cm^2) and by field emission scanning electron microscopy (FESEM).

Glass coverslips coated with surfmers of the polymer candidates (EA-*co*-DMAEMA and EA-*b*-DMAEMA) were placed on the bottom of the wells of a 24-well plate, and each well filled in with 2 mL of bacterial suspension (OD_{600} 0.1) in tryptic soy broth (TSB) + 1% glucose (w/v). The plate was incubated for 18 h at 37 °C after which time, the bacterial suspension was discarded, and glass coverslips were washed three times with PBS, to remove loosely adherent cells. CFU counts: the glass coverslips were collected into 15 mL-centrifuge tubes with 2 mL of PBS. Cells growing as a biofilm were detached by 10 min-soft sonication and 30 s vortexing. Six 10-fold dilutions were prepared, and 100 μL aliquots of each dilution were plated on Muller Hinton (MH) agar plates. CFUs were counted after overnight incubation at 37 °C, and CFUs per polymer surface unit were determined. FESEM analysis: the polymer coated coverslips with biofilm grown on the top were fixed with 2.5% glutaraldehyde in 0.1 M cacodylate buffer at room temperature for 1 hour and washed twice with 0.1 M cacodylate buffer. Sample dehydration was performed by ethanol/water solutions (30%, 50%, 70%, 85%, 95% and 100% v/v), 10 min each step and two repetitions with 100% (v/v) ethanol, and then by 1 : 1 ratio ethanol/hexamethyldisilazane (HMDS) solution for 4 min. Lastly, they were treated with 100% HMDS for 5 min, fixed with silver print on aluminium stubs and gold-coated by an

automatic sputter coater (Quorum Q150R S). Samples were examined by a field emission scanning electron microscope (Sigma-Zeiss) at an accelerating voltage of 4 kV.

Antimicrobial activity (EA-*b*-DMAEMA and EA-*co*-DMAEMA). *S. aureus* CH 10850 MRSA strain was cultured at 37 °C in aerobic conditions on a tryptic soy agar (TSA) plate, and few colonies were inoculated in 5 mL of TSB under shaking at 280 rpm until optical density $(OD)_{600}$ = 0.5 was reached. Distinct 10-fold dilutions of the culture (OD_{600} = 0.05) were prepared in TSB. These dilutions in TSB were grown at 37 °C with shaking at 280 rpm in absence (positive control) or presence of EA-*co*-DMAEMA and EA-*b*-DMAEMA compounds at different concentrations (2 mg mL^{-1}, 0.2 mg mL^{-1}, 0.02 mg mL^{-1}, and 0.002 mg mL^{-1}). The growth of all the cultures were monitored over time by measuring the increase in the respective $(OD)_{600}$ every 30 min for 3.5 h. Several blanks were prepared by using an equal volume of tryptic soy broth with the two polymers at the same explored concentrations (2 mg mL^{-1}, 0.2 mg mL^{-1}, 0.02 mg mL^{-1}, and 0.002 mg mL^{-1}) with no bacteria culture.

Simultaneously, 100 μL of every sample, at each time point, was serially diluted, and 100 μL of selected dilutions were spotted on MH plates and incubated overnight at 37 °C in duplicate. CFUs grown on MH plates were counted to determine the number of viable bacterial cells present within each culture.

Statistical analysis

In the statistical data analysis (as stated in the text) column represents mean values and error bars represent standard deviation (SD). Microparticle characterisation involved N = 1, n = 3 on a total number of 100 MPs analysed; biological characterisation involved N = 3, $n \geq 3$ biologically independent samples.

Results and discussion

Thiol-mediated free radical polymerisation (TFRP) was used to synthesise low molar mass (MWt) homo- and statistical copolymers (*i.e.*, <20 000 g mol^{-1}) that contained a target 20 mol% DMAEMA content. Benzyl mercaptan (BzSH) was used as model thiol chain transfer agent (CTA) because its aromatic group allowed for accurate polymer analysis *via* ^{1}H-NMR. Meanwhile, the synthesis of a block copolymer was achieved by sequential addition of DMAEMA to the EA macromonomer in an atom transfer radical polymerisation (ATRP; Scheme 1).

The chemical properties of the final copolymer materials synthesised in this study are reported in Table 1.

The TRFP polymers (Table 1, entry 1–4) exhibited relatively low M_n values, between 6000 and 13 000 g mol^{-1}, which confirmed that the quantity of CTA employed (1 mol% with respect to the monomers) was sufficient to deliver the required control over the chain lengths. Also, the dispersity values ($Đ$) were noted to be between 1.3 and 1.8, which are typical for a 'well-controlled' TFRP.[39] Additionally, in the statistical copolymer (entry 1), the comonomer ratio was found to have reached the desired 20% DMAEMA.

Table 1 Calculated EA : DMAEMA ratios M_n and $Đ$ data for the synthesised homopolymer and statistical (EA-*co*-DMAEMA) and block (EA-*b*-DMAEMA) surfactants

Entry	Polymers	M_n (g mol^{-1})	$Đ$	Final copolymer ratio[d] (% mol/mol)
1	EA-*co*-DMAEMA[a]	13 100[c]	1.3[c]	80 : 20
2	PolyEA[a]	8900[c]	2.2[c]	—
3	PolyDMAEMA[a]	6000[e]	n/a[e]	—
4	EA-*b*-DMAEMA[b]	15 700[c]	1.2[c]	91 : 8

[a] TRFP. [b] ATRP. [c] M_n and $Đ$ were obtained *via* permeation chromotography (GPC) using THF as eluent. [d] Final copolymer ratios were calculated by ^{1}H-NMR. [e] The M_n of polyDMAEMA was calculated *via* ^{1}H-NMR because the GPC chromatogram was influenced by an interaction between the amino groups and the stationary phase.

Meanwhile, the synthesis of a block copolymer typically required the use of two step polymerisation. The first step included the synthesis of a macroinitiator (*i.e.*, the reactive first block), from which the second block was subsequently grown. In this study, a poly(EA) macroinitiator was prepared following the synthetic procedure developed by Datta *et al.*,[37] from which the DMAEMA block was grown. The ATRP was conducted in bulk using EBriBru as the initiator and the combination of PMDETA/Cu(I)Br as catalyst. The target theoretical M_n was 13 000 g mol^{-1}, to deliver a similar molar mass to those obtained with the random copolymers. The products M_n was recorded as 13 190 g mol^{-1} with a $Đ$ of 1.12 (Fig. 1). The subsequent polymerisation of the DMAEMA second block was performed in acetone using a Cu(I)Cl:Cu(II)Cl:HMTETA complex as catalyst at 50 °C. The ^{1}H-NMR and GPC data (Fig. 1) in Table 1 also demonstrated that, for the EA-*b*-DMAEMA copolymer, the second block of DMAEMA had successfully grown from the EA block. The chemical shifts attributed to the DMAEMA side chain could be observed in the EA-*b*-DMAEMA block copolymer ^{1}H-NMR spectra in Fig. 1, confirming the presence of this monomer in the copolymer structure and allowed the monomer (EA/DMAEMA) ratio to be calculated. In addition, the GPC traces (Fig. 1) show a slight shift from the EA macromonomer to the block copolymer, evidencing the growth of the second block. However, the unexpected bimodal nature of this chromatogram was attributed to an interaction between the DMAEMA block and the gel of the column. Similarly, the molar mass of the homopolymer polyDMAEMA was estimated from the ^{1}H-NMR data alone since no traces in the GPC could be observed (Table 1, entry 3).

Whilst the relative feed DMAEMA to macroinitiator molar ratios were theoretically required to reach the target 20% mol DMAEMA content, the actual comonomer final product molar ratio achieved was very close to 90 : 10 mol% : mol% EA : DMAEMA, which was enough to produce stable self-assembling.

Investigation of 3D surfmer surface characteristics *via* microparticle production with EA-*co*-DMAEMA and EA-*b*-DMAEMA copolymers

The same oil-in-water (O/W) droplet flow-focusing chip microfluidic system adopted in previous studies was used with both

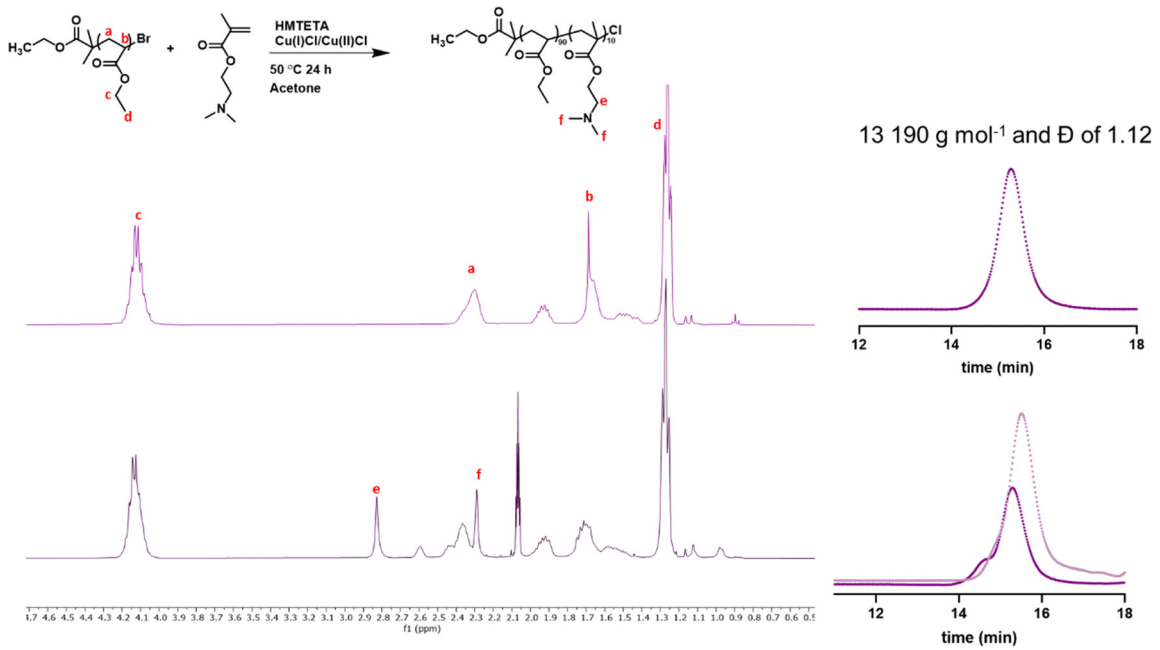

Fig. 1 Scheme of reaction for EA-*b*-DMAEMA. Top: ^{1}H-NMR spectra and aligned GPC chromatogram of poly(ethyl acrylate) and bottom: ^{1}H-NMR spectra and the respective GPC chromatograms of the block copolymers EA-*b*-DMAEMA.

the block and statistical surfmers to determine their suitability to act as surfactants for the preparation of microparticles (MP).[14,40] The dispersed feed stream contained these novel amphiphilic copolymers (2% w/v), a photoinitiator (2% w/v) and 1,6-hexanediol diacrylate (HMDA, 96% w/v) as a core material. The flow rates through the chip of both the dispersed and the continuous phase (water) were optimised to ensure the formation of stable and monodisperse particles. When changing the flow rates of the dispersed phase (Q_d) and continuous phase (Q_c), different flow regime profiles can be observed within the channels (*e.g.*, dripping, wall wetting, jetting, unstable particle, satellites formation and squeezing), which can affect the performance of the MPs manufacturing process.[14] Fig. S1 (ESI†) contains the flow diagrams of the EA-*co*-DMAEMA and EA-*b*-DMAEMA surfactants at a chosen concentrations, which were built by systematically varying the Q_d and the Q_c from 0.1 mL h^{-1} to 0.5 mL h^{-1} and from 1 mL h^{-1} to 9 mL h^{-1}, respectively. Both surfactants displayed similar gradual flow regime changes as the flow rate conditions were altered, with the increasing of Q_d and Q_c, passing through the main four different flow behaviours: wetting, squeezing, dripping, and jetting. This systematic study demonstrated that both copolymer types formed stable emulsions under the appropriate flow conditions and thus their capability to behave as surfactants. Fig. 2a and b contains the microfluidic particle sizing data and the SEM images of the resulting MPs at 250× and 650× resolution for both surfactants. The conditions under which the block and statistical materials exhibited formation of stable droplets (inside the channels of the microfluidic chip), were found to be similar with both producing a stable emulsion within the flow window of Q_c 4–6 mL h^{-1} and Q_d 0.1–0.2/0.3 mL h^{-1}. The data in Fig. 2a demonstrated that the MPs generated were spherical with a diameter (60–70 μm) lower than the orifice width (100 μm), highlighting the efficiency of the surfactant in stabilising the interface between the two phases. The EA-*co*-DMAEMA seemed to perform less well as a surfactant, exhibiting a higher CV of 9% and a larger size distribution range of ∼60 to ∼70 μm, than the EA-*b*-DMAEMA (Fig. 2a). This indicated that the molecular surface arrangement of the two surfmers may be different, due to their differing 3D architectures. In the case of the statistical surfmer, this data indicated that the stabilisation given by the charged amine residues (short pendent group length) were not as effective at stabilising the interface as the previously used longer pendant group PEGMA hydrophiles as shown in previous works (%CV in the range of 2.5–3.5).[14,23,40] However, such PEG-based hydrophiles could not be utilised in this study as they are known to prevent protein adhesion to surfaces.[41]

Meanwhile, with the EA-*b*-DMAEMA microparticles, the SEM analysis also indicated: (a) the appearance of pores on the surface and (b) that they were approximately 10 μm in diameter smaller than the statistical equivalents. Both observations were attributed to a difference in surfmer molecular surface orientation, suggesting that the block copolymer occupied a lower surface area between the particle and water interface. Its partitioned structure allowing it to orientate to be more perpendicular to the interface, with the DMAEMA block towards water and the EA extending towards the core. By comparison, the random structure of the EA-*co*-DMAEMA's backbone will force it to locate parallel to the interface due to the random distribution of the hydrophilic DMAEMA along its length. As a result, the EA-*b*-DMAEMA will cover less surface area per molecule, suggesting that an increased concentration of surfmer may be required to completely cover the surface and remove this

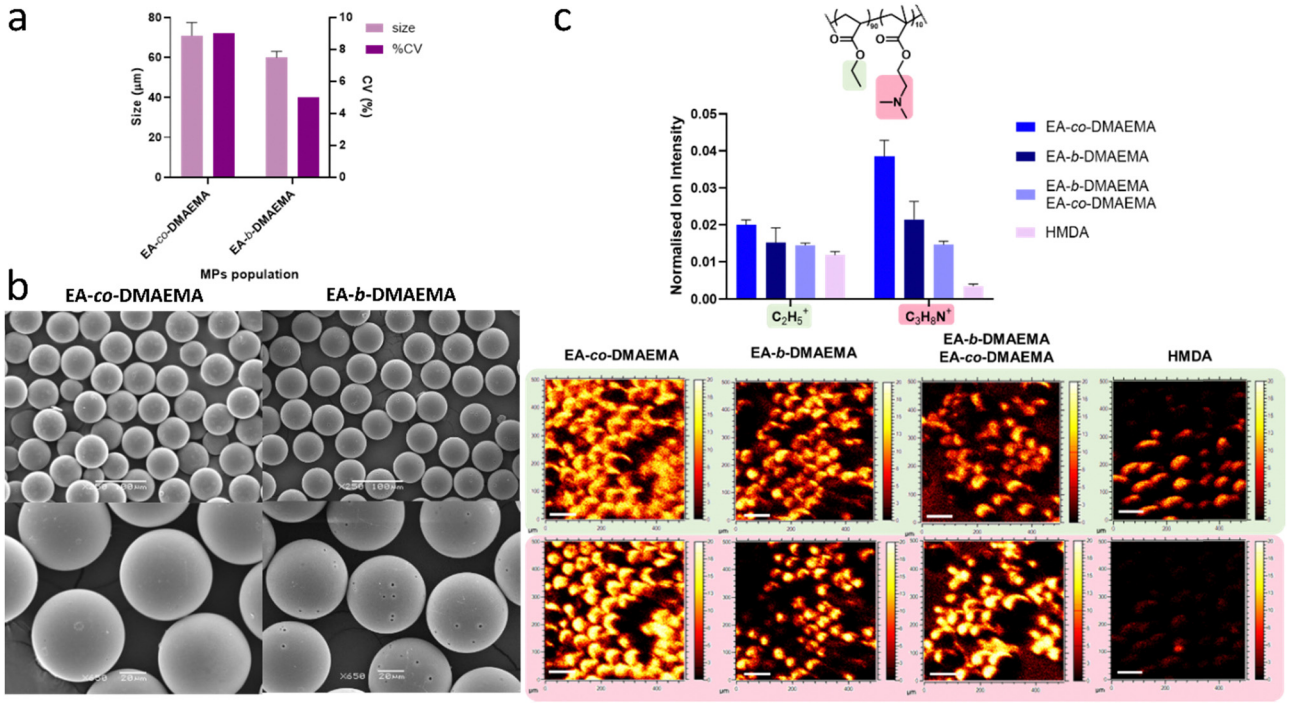

Fig. 2 Investigation of 3D surfmer surface characteristics *via* microparticle production with EA-*co*-DMAEMA and EA-*b*-DMAEMA copolymers: (a) plot of particle diameter and the coefficient of variation (%) for the EA-*co*-DMAEMA and EA-*b*-DMAEMA surfactants (N = 1, n = 3 total population analysed 100 MPs; error bars represent SD) produced by analysing the representative SEM images (b) SEM images of the polymer MPs (scale bars for upper figures is 100 μm with magnification of 250×; scale bars for the bottom figures is 20 μm with magnification of 650×) (c) ToF-SIMS data showing intensities and the related images of the key ions associated with both EA:DMAEMA copolymers within the surfmer structure at the surface of the MPs compared to the intensity of the same ions present in the core HMDA MPs spectra (ToF-SIMS images of key ions with y and x axes ranging from 0 to 500 μm. The intensity bar spans from 0 to 20 AU, and the scale bar represents 100 μm).

porosity. However, this proposed change in the orientation of the block surfmer, instead produced MPs that are monodisperse with a CV around 5%. This was attributed to (a) better polymer packing at the interface due to their perpendicular orientation and (b) the block nature of the steric footprint of the DMAEMA in the EA-*b*-DMAEMA, which resulted in the introduction of steric, as well as charge, stabilisation into the system. However, this steric block hydrophile may also, partially, explain the appearance of the microparticle surface porosity with the increase in hydrophile size concentrated in one area of the molecule leading to increased detachment from the interface prior to polymerisation. To investigate whether pore size might affect cell behaviour and/or fibronectin coating, SEM analysis was conducted on the pores. This estimated the average diameter to be 1.75 ± 0.24 μm. By comparison, the average size of the 3T3 fibroblasts used in this study, when rounded, is in the region of 10 μm, and, when it is spread, this value would be of the order of 100 μm. Thus, the pores are one to two orders of magnitude smaller than both the rounded and spread cells respectively. In addition, Chung *et al.* reported that fibroblast persistence time was unaffected by the presence of pores, although the cells did exhibit directionality preferences based on pore patterning. So, as our SEM images revealed a random pore distribution, we therefore believe that the porosity of the microparticles produced will not significantly affect cell behaviour.

Finally, similar surface or self-assembly behaviour has been previously reported in other end-use applications such as: micro/nanofabrication of functional materials, the formation of polymersomes and in energy storage/conversion which support the self-assembly conclusions made by the authors.[42,43]

Microparticle surface characterisation

Time of flight secondary ion mass spectrometry (ToF-SIMS) analysis was used to investigate the bio-instructive surface characteristics of the microparticles, and to investigate how this was dictated by the surfmers used to produce the MPs. The data was collected in both positive and negative ion mode to identify unique ions associated with the hydrophilic and hydrophobic moieties within the copolymers. For these copolymers, the unique identifier found for the DMAEMA molecular structure was the $C_3H_8N^+$ ion, whilst the $C_2H_5^+$ was most associated with EA moieties. However, due to the simplicity of the EA structure, there is a small possibility that this ion can also be generated in very small quantities from the DMAEMA. Fig. 2c bar graph represents the total ion counts for the MPs produced using each copolymer alone and a mixed surfmer system containing both surfmers and HMDA core only particles (*i.e.*, MPs prepared without the aid of a surfmer to demonstrate the difference between the unfunctionalized and functionalised MPs).

From Fig. 2c, it was possible to confirm the presence of the surfmers on the MPs surfaces thanks to the presence of the

detection of the characteristic ion of DMAEMA moieties ($C_3H_8N^+$) within the structure. The MPs controlled by EA-*b*-DMAEMA exhibited the highest levels of the unique DMAEMA ion ($C_3H_8N^+$) of all the samples containing the copolymers. This ion was also found at the surface of both the EA-*co*-DMAEMA MP's and mixed surfmer samples, but it was more diffusely distributed across the surface when compared to the microparticles prepared using the block copolymer where the individual shape of each MPs could be clearly defined. Again, this was proposed to support the conclusion that the orientation of the block copolymer is different to that of the statistical surfmer. Finally, the intensity for this ion is very low on the HMDA core/no surfactant MP, which was expected as there is no DMAEMA in/on the sample.

Investigation of 2D surfmer surface characteristics *via* the production of EA-*co*-DMAEMA statistical and EA-*b*-DMAEMA block copolymers surface deposited films

As the confirmation of surface structure at the MP surface was complex due to the 3D nature of the MPs, 2D samples were produced to confirm that different surface conformations were exhibited by these two copolymer architectures. This was achieved by dip-coating glass slides with samples of EA-*b*-DMAEMA, EA-*co*-DMAEMA, polyDMAEMA and polyEA copolymer and subjecting these to ToF-SIMS analysis. In Fig. S2a and b (ESI†), the $C_2H_5^+$ ion exhibited high intensities in the polyEA homopolymer film and, as expected, was also found to present in the DMAEMA film in trace amounts. Similarly, again as expected, the $C_3H_8N^+$ ion is totally absent from the polyEA sample. Meanwhile, in the case of 2D films when contrasting the intensities of the $C_3H_8N^+$ ion exhibited in films of the block and random copolymers, it was noted that these varied dramatically. The EA-*co*-DMAEMA coating exhibited intensities from both $C_2H_5^+$ and $C_3H_8N^+$ ions, suggesting that the random architecture allowed both chemistries to orientate towards the "outer" surface *i.e.* the coating: biology surface. This was similar to the behaviour that was observed with the surface of the MPs in Fig. 2c. Meanwhile, the block copolymer data did not show any intensity for the DMAEMA identifier ion. Thus, it was hypothesised that the DMAEMA block was more attracted to the hydrophilic surface of the coverslip, containing OH groups, and so it had arranged itself to face towards the "inner" coating: glass surface only. Thus, the DMAEMA was, in effect, anchoring the block copolymer to the surface. This potentially suggesting an additional benefit of these block structures, namely that the DMAEMA block may, due to its size and high local concentration of amino functionality, provide a better anchor onto the surface of the glass so giving an increased resistance to the coating delaminating. Consequently, the block copolymer will only then present the EA block towards any solution that is it placed into. As a result, the surface will appear to be similar to the polyEA homopolymer. In fact, for films of block copolymers or polymer blends containing chemically distinct components, it is well known that differences in the surface energies of the components can lead to a variety of surface-related phenomena, including surface-induced ordering and orientation.[44–47] This observation also supported the conclusions drawn on the trends in surface available functionality observed for the functionalised MPs, which suggests that the orientation of each block is driven by the affinity with the surrounding environment and its surface energy based on its chemical nature (*i.e.*, hydrophobic and/or hydrophilic *etc.*).[48] Therefore, the perpendicular orientation of the block copolymer in an oil in water emulsion will lead to the dominance of the DMAEMA block copolymer on the surface.

Effect of surfmer orientation on biological performance

After assessing the difference in surface orientation of the hydrophilic/hydrophobic moieties, the polymer coated coverslips were tested *in vitro* for the attachment and viability of mammalian and bacterial cells. The ability of 3T3 fibroblast cells to adhere on 2D coverslips coated with polyEA, EA-*co*-DMAEMA and EA-*b*-DMAEMA (but without FN adsorption) was conducted using LIVE/DEAD™ staining and their viability assessed using the Presto Blue assay (Fig. 3a and b). Similarly, the biofilm-forming ability of *S. aureus* (CH 10850) was evaluated on 2D glass coverslips coated with EA-*co*-DMAEMA and EA-*b*-DMAEMA. In this experiment, after incubation, bacterial cells adhered onto the glass slides were detached, counted (Fig. 3c) and observed by FESEM (Fig. 3d). Additionally, bacterial cell viability after 3.5 h of incubation with the different surfmer solutions was observed (Fig. 3e).

Based on the observations from data shown in Fig. 3a and b, the tested materials were not cytotoxic to 3T3 fibroblasts, except for the random copolymer (EA-*co*-DMAEMA).[48] On the EA-*b*-DMAEMA surface, the FN nanonetwork is visible suggesting that the presence of the EA block has favoured its organisation. This observation further supports our findings from the mammalian cell adhesion experiments. Proposed mechanisms for the cytotoxicity of DMAEMA based copolymers have been reported to be very dependant of both molecular weight and copolymer ratio. For example, Knetsch *et al.* prepared a series of copolymers containing DMAEMA and MMA in various molar ratios and evaluated the toxicity of both any leachate from the materials and the washed surface.[49] They reported that the measured toxicity increased with increasing DMAEMA content. Immuno-staining for phospho-tyrosine or vinculin demonstrated gradual loss of focal adhesions on the increasingly toxic surfaces. The loss of focal adhesions was found to coincide with an increase in paxillin and vinculin protein, indicating cells try compensating for loss of adhesion.

Meanwhile, a high throughput study of DMAEMA copolymers by Weiss *et al.* synthesized 107 copolymers which varied in charge, hydrophobicity, and molecular weight, and screened them for both cytotoxic behaviour and immunogenic responses.[50] They identified the following three compositional regions of interest: (a) highly cationic polymers which disrupted the cellular plasma membrane to induce a toxic phenotype, (b) high molecular weight, hydrophobic polymers which were taken up by the cell *via* active transport to induce an immunogenic phenotype and (c) tertiary amine- and triethylene glycol-containing polymers that did not invoke immunogenic or toxic responses which they

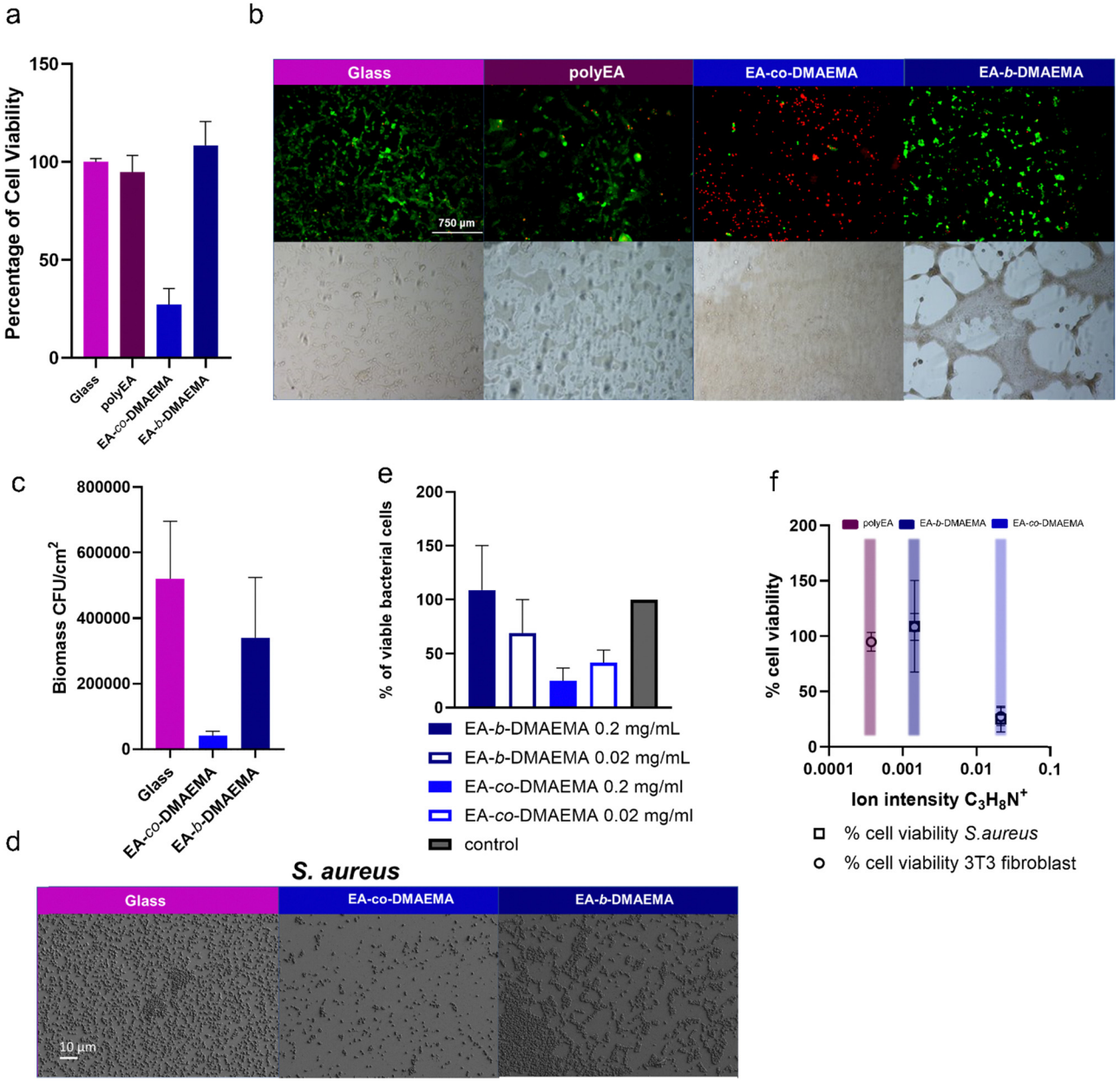

Fig. 3 Effect of surfmer orientation on mammalian 3T3 fibroblast cell attachment and viability, bacterial (*S. aureus*) biofilm formation, and on fibronectin attachment and molecular orientation. (a) Mammalian cell viability of 3T3 fibroblasts following 24-hour incubation on 2D coated coverslips as measured using the Presto Blue assay (n = 3, error bars represent SD; viability expressed as percentage of the glass control). (b) Representative fluorescence images illustrating cell adhesion and viability on the 2D coated coverslips using the Live/Dead assay (Calcein-AM LIVE, GREEN) and propidium iodide (PI – DEAD, RED; scale bar 750 µm); merged fluorescence images shown with the corresponding phase contrast images. Scale bar 750 µm. (c) Biomass quantification after incubation of *S. aureus* (CH 10850) for 18 h at 37 °C on glass coverslips dip coated with the polymer candidates surfmers (EA-*co*-DMAEMA and EA-*b*-DMAEMA). Cell numbers are expressed as a CFU per polymer surface unit (n = 3, N = 1; error bars represent SD) (d) FESEM micrographs of bacterial adhesion on control (glass), EA-*co*-DMAEMA and EA-*b*-DMAEMA. Scale bar 10 µm. (e) % of viable cells of *S. aureus* (CH 10850) following incubation with the polymer surfmers (EA-*co*-DMAEMA and EA-*b*-DMAEMA) at two different concentrations (0.2 mg mL^{-1} and 0.02 mg mL^{-1}). CFUs grown on MH plates were counted to determine the number of viable bacterial cells present within each culture. (f) Correlation between $C_3H_8N^+$ intensity obtained from Fig. S2a (ESI†) against % cell viability from both *S. aureus* and 3T3 fibroblast.

attributed to a combination of their pK_a values and high degrees of charge shielding conferred from ethylene glycol moieties. Previous studies have shown that these characteristics could prevent rupture of membranes and facilitate safe, intracellular delivery when complexed with RNA.[51,52] Consequently, in this study, we avoided high levels of DMAEMA (molar ratio always less or equal to 20%) and high molecular weight (our copolymer M_n's raged from ~6000 to 16 000 g mol^{-1}) to avoid these potential toxicity triggers. Furthermore, whilst the Knetsch study suggests that lack of surface adhesion may play a role in DMAEMA based toxicity, this work

would suggest that this may not be the case with all copolymers, as in this study there was significant FN adhesion, but a toxic response was still induced.[49]

To further emphasize the influence of surface properties on biological behaviour, glass slides coated with the surfmers bearing cationic functionality were tested against a Gram-positive microorganism, *S. aureus*, in order to determine their anti-biofilm efficacy with respect to non-coated (control) glass coverslips after 18 h incubation. The FESEM images in Fig. 3d demonstrated that *S. aureus* adhered to both the control and EA-*b*-DMAEMA coated surfaces, whereas adhesion was significantly reduced on the EA-*co*-DMAEMA surface. This finding was supported by the values of adhered biomass (CFU per cm^2) shown in Fig. 3c, indicating lower biomass amount on the random copolymer EA-*co*-DMAEMA compared to the control and the second tested material (EA-*b*-DMAEMA). Additionally, antimicrobial tests were also performed on bacterial cells in planktonic mode of growth. Incubation with the test polymer EA-*co*-DMAEMA resulted in killing of bacterial cells during the exponential growth at both concentrations tested (Fig. 3e), similar to the cytotoxicity observed in the experiments carried out on mammalian cells (Fig. 3a). Cationic polymers have been known to possess inherent antimicrobial activity due to their net positive charge, particularly against Gram-positive bacteria.[53] The mechanism of action for this class of polymers involves the binding of the agent to the cell wall through electrostatic interactions, thus affecting membrane permeability and finally leading to membrane lysis.[53–55]

These findings corroborate the observations made during the chemical-surface characterization of the polymers using ToF-SIMS which indicated surface-induced ordering and orientation of the DMAEMA side chain at the surface depending on the surfmers architecture. Interestingly, a correlation between $C_3H_8N^+$ intensity against % cell viability from both *S. aureus* and 3T3 fibroblasts (Fig. 3f) showed how the surface is affecting the biological responses in a similar manner. In fact, in the surfaces where the $C_3H_8N^+$ intensity is low (polyEA and EA-*b*-DMAEMA), both mammalian and bacterial cells showed low toxicity. On the other hand, when EA-*co*-DMAEMA was at the surface, the ion uniquely identifying DMAEMA gave the highest intensity corresponding to the killing effect in both experiments.

Based on the authors experience,[13–15,23,33] the crucial factor that has been used to predict/design the bio-instructive biological results discussed in this study was related to the molecular pendant group moieties that are prominent on the surface of the coating/nanoparticles. Consequently, in the previous publications, we have reported that statistical copolymers could be used to deliver two types of biological surface influence, *e.g.* (a) biofilm attachment resistance and/or (b) anti-swarming behaviour.[56] This ''composite'' behaviour has been shown to be as a direct result of the copolymer structures ensuring that both desired bio-instructive moieties are present at the surface.

Meanwhile, in this study, we report a key novelty of adopting a block rather than statistical copolymer structure such that a copolymer coating is derived that presents only one of the copolymer functional pendant moieties at the surface of the coating/nanoparticles. Thus, for the first time, this type of bio-instructive coating has been observed to act as a homo-polymer of only one of the copolymer components. Thus, it was concluded from the corroborating evidence of both the surface chemistry analysis using TOF-SIMS and the subsequent biological assay results, that the block copolymer is surface assembling to present this single functionality. The conclusion is supported by the fact that the DMAEMA-*co*-EA statistical copolymer presents both copolymer functionalities at the surface showing that a non-surface assembled polymer will not present a homo-EA surface.

Effect of ethyl acrylate chemistry orientation on fibronectin network

Fibronectin fibrillogenesis, a pivotal cell-mediated process driven by integrin activation, instigates conformational alterations in fibronectin molecules and orchestrates the organization of the actin cytoskeleton.[32,33,54] It was previously shown that certain chemistries, such as polyethylene amine (PEA), can induce a similar process in the absence of cells. This chemical stimulation augments fibronectin–fibronectin interactions, ultimately giving rise to the formation of a highly potent and biologically active network.[32,33,54] Alternatively, in the present study, we investigated the impact of introducing additional moieties to the ethyl acrylate polymer chain on the assembly of fibronectin networks. By doing so, we aimed at expanding the utility of ethyl acrylate, rendering it capable of being manufactured as a surfactant in addition to inducing a biological effect through fibronectin assembly. This strategy could result as a promising avenue for the design and fabrication of enhanced surfactant materials with application in regenerative medicine. We studied the adhesion and cell viability of 3T3 fibroblast mammalian cells on coverslips coated with polyEA, EA-*co*-DMAEMA and EA-*b*-DMAEMA after adsorption of FN from human plasma at the concentration of 20 μg mL^{-1} (Fig. 4) to assess the cytocompatibility of the materials and their ability to support mammalian cell adhesion.

Our findings from Fig. 4a and b demonstrate that, in general, the tested materials are able to support mammalian cell adhesion and are not cytotoxic, with the exception of the random copolymer, EA-*co*-DMAEMA. Interestingly, fibronectin adsorption did not improve the viability of the cells when cultured on the EA-*co*-DMAEMA coated surface. It is important to note that the 70 kDa amino terminal regions of fibronectin are crucial for cell-mediated assembly and conferring FN binding activity. Within this region, FN binding activity determines the ability of FN to bind to surfaces.[55] The presence of a positive charge on the surface, in the random copolymer, may have caused a repulsion effect, leading to no adsorption of FN on the surface. Furthermore, as the fibrillogenesis of FN on polyEA has been extensively studied by Llopis-Hernandez *et al.*, demonstrating its significant role in promoting FN organization,[32] we investigated the organization of FN at the material interface on the two, novel different chemistries synthesised in this study: EA-*co*-DMAEMA and EA-*b*-DMAEMA. AFM images (Fig. 4c) of

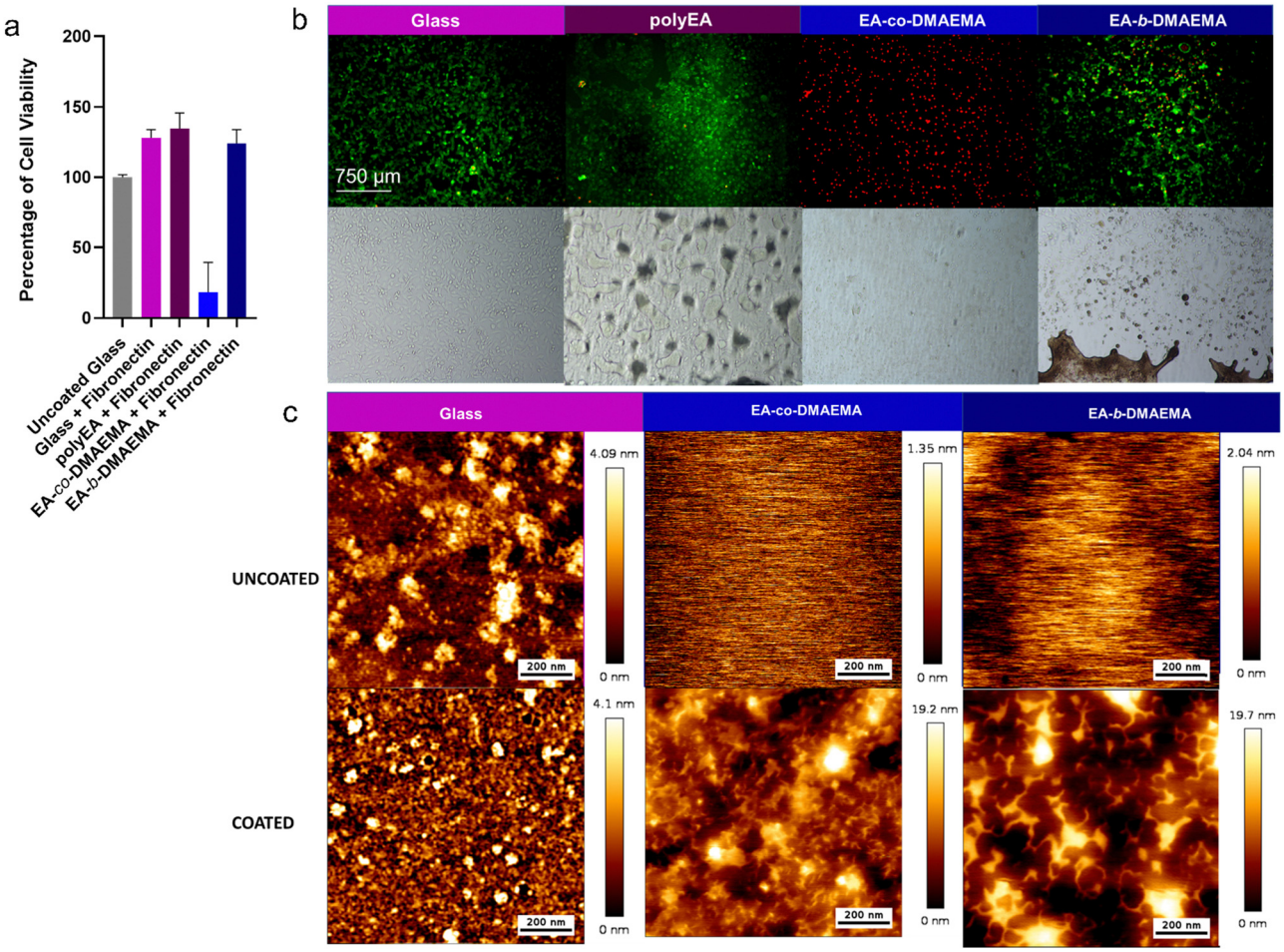

Fig. 4 Effect of ethyl acrylate chemistry orientation on fibronectin network assembly and on subsequent mammalian 3T3 fibroblast adhesion and viability: (a) mammalian 3T3 fibroblast viability on various coated glass coverslips and following fibronectin adsorption using the Presto Blue viability assay expressed as a percentage of the control (cells on uncoated glass) (data is presented as means ± SD; n = 3). (b) Representative fluorescence (Live/Dead™ stain: Calcein-AM (LIVE, GREEN) and propidium iodide (PI – DEAD, RED) and light microscopy images of 3T3 fibroblasts cultured on glass (control), polyEA, EA-*co*-DMAEMA and EA-*b*-DMAEMA coated surfaces (n = 3 N = 1). Scale bar 750 µm. (c) Atomic force microscopy (AFM) images after FN coating on plain glass coverslips and EA-*co*-DMAEMA and EA-*b*-DMAEMA coated coverslips. The intensity bar spans from 0 to 20 AU, and the scale bar represents 200 nm.

the plain glass coverslip and polymer coated surfaces, in the absence of FN, do not show any characteristic feature. After the FN adsorption (Fig. 4c), the plain glass and EA-*co*-DMAEMA surfaces show the typical globular FN conformation, indicating the absence of substrate-induced fibrillogenesis. On the EA-*b*-DMAEMA surface, the FN nanonetwork is visible suggesting that the presence of the EA block has favoured its organisation. This observation further supports our findings from the mammalian cell adhesion experiments.

Conclusions

This study successfully synthesized two PEG-free amphiphilic copolymers: a statistical copolymer (EA-*co*-DMAEMA) and a block copolymer (EA-*b*-DMAEMA) using TFRP and ATRP, respectively. Both possessed the desired low molar mass and exhibited good characteristics for use as microparticle surface modifiers. However, the block copolymer (EA-*b*-DMAEMA) demonstrated superior performance in several key aspects. It produced monodisperse microparticles with smaller sizes and lower coefficient of variation compared to the statistical copolymer. ToF-SIMS analysis confirmed a preferential orientation of the DMAEMA block at the microparticle interface, suggesting superior surface enrichment compared to the random copolymer. Unlike the cytotoxic statistical copolymer, the block copolymer (EA-*b*-DMAEMA) exhibited excellent mammalian cell biocompatibility and promoted fibronectin network formation, suggesting great potential for regenerative medicine applications. In addition, the surface induced-ordering orientation of DMAEMA depending on surfmers architecture resulted in killing of bacterial cells with EA-*co*-DMAEMA, and subsequently, low biofilm formation. Interestingly, a correlation between $C_3H_8N^+$ intensity against % cell viability from both *S. aureus* and 3T3 fibroblasts showed how the surface is affecting the biological responses. In fact, in the surfaces where

DMAEMA is less exposed to the external environment (polyEA and EA-*b*-DMAEMA), both mammalian and bacterial cells showed low toxicity. By strategically arranging the monomer sequence (statistical *vs.* block), we can achieve superior control over surface properties and functionality, promoting advanced materials in drug delivery, tissue engineering, and other biomedical fields and highlighting the importance of copolymer architecture in material design.

Data availability

The data supporting this article have been included as part of the ESI.†

Conflicts of interest

There are no conflicts to declare.

Acknowledgements

This work was supported by the Engineering and Physical Sciences Research Council [grant numbers EP/N006615/1 and EP/P001114/1] and the UKRI funded UK Regenerative Medicine Platform 2 – Acellular Hub (MR/R015651/1).

References

1 N. C. T. Dadi, B. Radochová, J. Vargová and H. Bujdáková, *Microorganisms*, 2021, **9**, 2332.
2 X. Zhao, Q. Li, Z. Guo and Z. Li, *Stem Cell Res. Ther.*, 2021, **12**, 1–13.
3 K. Sadtler, A. Singh, M. T. Wolf, X. Wang, D. M. Pardoll and J. H. Elisseeff, *Nat. Rev. Mater.*2016, **1**, 16040.
4 F. Batool, H. Özçelik, C. Stutz, P. Y. Gegout, N. Benkirane-Jessel, C. Petit and O. Huck, *J. Tissue Eng.*, 2021, **12**, DOI: 10.1177/20417314211041428.
5 L. M. Weiner, A. K. Webb, B. Limbago, M. A. Dudeck, J. Patel, A. J. Kallen, J. R. Edwards and D. M. Sievert, *Infect. Control Hosp. Epidemiol.*, 2016, **37**, 1288–1301.
6 A. M. C. Maan, A. H. Hofman, W. M. de Vos and M. Kamperman, *Adv. Funct. Mater.*, 2020, **30**(32), 2000936.
7 T. Tolker-Nielsen, *Microbiol. Spectrum*, 2015, **3**, 1–12.
8 A. Cassini, L. Diaz Högberg, D. Plachouras, A. Quattrocchi, A. Hoxha and G. Skov Simonsen, *et al.*, *Lancet Infect. Dis.*, 2019, **19**, 56–66.
9 A. H. Holmes, L. S. P. Moore, A. Sundsfjord, M. Steinbakk, S. Regmi, A. Karkey, P. J. Guerin and L. J. V. Piddock, *Lancet*, 2016, **387**, 176–187.
10 Y. Cheng, G. Feng and C. I. Moraru, *Front. Microbiol.*, 2019, **10**, 1–17.
11 T.-F. C. Mah and G. A. O'Toole, *Trends Microbiol.*, 2001, **9**, 34–39.
12 C. De la Fuente-Núñez, F. Reffuveille, L. Fernández and R. E. W. Hancock, *Curr. Opin. Microbiol.*, 2013, **16**, 580–589.
13 V. Cuzzucoli Crucitti, L. Contreas, V. Taresco, S. C. Howard, A. A. Dundas, M. J. Limo, T. Nisisako, P. M. Williams, P. Williams, M. R. Alexander, R. D. Wildman, B. W. Muir and D. J. Irvine, *ACS Appl. Mater. Interfaces*, 2021, **13**, 43290–43300.
14 A. A. Dundas, V. Cuzzucoli Crucitti, S. Haas, J. Dubern, A. Latif, M. Romero, O. Sanni, A. M. Ghaemmaghami, P. Williams, M. R. Alexander, R. Wildman and D. J. Irvine, *Adv. Funct. Mater.*, 2020, **30**, 2001821.
15 A. L. Hook, C.-Y. Chang, J. Yang, J. Luckett, A. Cockayne, S. Atkinson, Y. Mei, R. Bayston, D. J. Irvine, R. Langer, D. G. Anderson, P. Williams, M. C. Davies and M. R. Alexander, *Nat. Biotechnol.*, 2012, **30**, 868–875.
16 H. J. Haugen, C. Soc Rev, M. Rahmati, E. A. Silva, J. E. Reseland and C. A. Heyward, *Chem. Soc. Rev.*, 2020, **49**, 5178.
17 A. Ranella, M. Barberoglou, S. Bakogianni, C. Fotakis and E. Stratakis, *Acta Biomater.*, 2010, **6**, 2711–2720.
18 Y. Zhang, H. Pan, P. Zhang, N. Gao, Y. Lin, Z. Luo, P. Li, C. Wang, L. Liu, D. Pang, L. Cai and Y. Ma, *Nanoscale*, 2013, **5**, 5919–5929.
19 Z. Chen, Y. Fan, L. Wang, Z. Bian and L. Hao, *RSC Adv.*, 2021, **57**, 36360–36366.
20 L. Wang, M. He, T. Gong, X. Zhang, L. Zhang, T. Liu, W. Ye, C. Pan and C. Zhao, *Biomater. Sci.*, 2017, **5**, 2416–2426.
21 A. J. Vegas, O. Veiseh, J. C. Doloff, M. Ma, H. H. Tam, K. Bratlie, J. Li, A. R. Bader, E. Langan, K. Olejnik, P. Fenton, J. W. Kang, J. Hollister-Locke, M. A. Bochenek, A. Chiu, S. Siebert, K. Tang, S. Jhunjhunwala, S. Aresta-Dasilva, N. Dholakia, R. Thakrar, T. Vietti, M. Chen, J. Cohen, K. Siniakowicz, M. Qi, J. McGarrigle, S. Lyle, D. M. Harlan, D. L. Greiner, J. Oberholzer, G. C. Weir, R. Langer and D. G. Anderson, *Nat. Biotechnol.*, 2016, **34**, 345.
22 L. Yang, S. Pijuan-Galito, H. S. Rho, A. S. Vasilevich, A. D. Eren, L. Ge, P. Habibović, M. R. Alexander, J. De Boer, A. Carlier, P. Van Rijn and Q. Zhou, *Chem. Rev.*, 2021, **121**, 4561–4677.
23 A. Latif, L. E. Fisher, A. A. Dundas, V. Cuzzucoli Crucitti, Z. Imir, K. Lawler, F. Pappalardo, B. W. Muir, R. Wildman, D. J. Irvine, M. R. Alexander and A. M. Ghaemmaghami, *Adv. Mater.*, 2022, **36**(43), 2208364.
24 P. V. Giannoudis, E. Jones and T. A. Einhorn, *Injury*, 2011, **42**, 549–550.
25 H.-S. Sohn and J.-K. Oh, *Biomater. Res.*, 2019, **23**, 9.
26 Y. Fillingham and J. Jacobs, *Bone Joint J.*, 2016, **98-B**, 6–9.
27 V. Campana, G. Milano, E. Pagano, M. Barba, C. Cicione, G. Salonna, W. Lattanzi and G. Logroscino, *J. Mater. Sci.: Mater. Med.*, 2014, **25**, 2445–2461.
28 H. S. Sohn and J. K. Oh, *Biomater. Res.*, 2019, **23**, 9.
29 G. Kumar and B. Narayan, *Classic Papers in Orthopaedics*, 2014, pp. 527–530.
30 R. Dimitriou, E. Jones, D. McGonagle and P. V. Giannoudis, *BMC Med.*, 2011, **9**, 66.
31 H. Donnelly, M. Salmeron-Sanchez and M. J. Dalby, *J. R. Soc. Interface*, 2018, **15**(145), DOI: 10.1098/RSIF.2018.0388.
32 V. Llopis-Hernández, M. Cantini, C. González-García, Z. A. Cheng, J. Yang, P. M. Tsimbouri, A. J. García, M. J. Dalby

and M. Salmerón-Sánchez, *Sci. Adv.*, 2016, **2**(8), DOI: 10.1126/sciadv.1600188.
33 M. Salmerón-Sánchez, P. Rico, D. Moratal, T. T. Lee, J. E. Schwarzbauer and A. J. García, *Biomaterials*, 2011, **32**, 2099–2105.
34 M. M. Martino and J. A. Hubbell, *FASEB J.*, 2010, **24**, 4711–4721.
35 M. Croes, B. C. H. van der Wal and H. C. Vogely, *J. Orthop. Res.*, 2019, **37**, 2067–2076.
36 M. Vassey, L. Ma, L. Kämmerling, C. Mbadugha, G. F. Trindade, G. P. Figueredo, F. Pappalardo, J. Hutchinson, R. Markus, S. Rajani, Q. Hu, D. A. Winkler, D. J. Irvine, R. Hague, A. M. Ghaemmaghami, R. Wildman and M. R. Alexander, *Matter*, 2023, **6**, 887–906.
37 H. Datta, A. K. Bhowmick and N. K. Singha, *Macromolecular Symposia*, John Wiley & Sons, Ltd, 2006, vol. 240, pp. 245–251.
38 J. Huang, B. Cusick, J. Pietrasik, L. Wang, T. Kowalewski, Q. Lin and K. Matyjaszewski, *Langmuir*, 2007, **23**, 241–249.
39 J. P. A. Heuts, L. M. Muratore and T. P. Davis, *Macromol. Chem. Phys.*, 2000, **201**, 2780–2788.
40 C. A. Henshaw, A. A. Dundas, V. C. Crucitti, M. R. Alexander, R. Wildman, F. R. A. J. Rose, D. J. Irvine and P. M. Williams, *Molecules*, 2021, **26**, 1–15.
41 E. A. Vogler, *Biomaterials*, 2012, **33**, 1201–1237.
42 S. B. Darling, *Prog. Polym. Sci.*, 2007, **32**, 1152–1204.
43 C. Pinto-Gómez, F. Pérez-Murano, J. Bausells, L. G. Villanueva and M. Fernández-Regúlez, *Polymers*, 2020, **12**, 2432.
44 H. Yokoyama, T. E. Mates and E. J. Kramer, *Macromolecules*, 2000, **33**, 1888–1898.
45 M. W. Matsen, *Curr. Opin. Colloid Interface Sci.*, 1998, **3**, 40–47.
46 J. Chen, X. Wang, S. R. Kline, S. Puri and H. L. Frisch, *J. Phys.: Condens. Matter*, 1997, **9**, 2109–2133.
47 X. Y. Lang, Y. F. Zhu and Q. Jiang, *Thin Solid Films*, 2006, **515**, 2765–2770.
48 S. H. Kim, M. J. Misner and T. P. Russell, *Adv. Mater.*, 2008, **20**, 4851–4856.
49 M. L. W. Knetsch, N. Olthof and L. H. Koole, *J. Biomed. Mater. Res., Part A*, 2007, **82**, 947–957.
50 A. M. Weiss, M. A. Lopez, B. W. Rawe, S. Manna, Q. Chen, E. J. Mulder, S. J. Rowan and A. P. Esser-Kahn, *Macromolecules*, 2023, **56**, 7286–7299.
51 F. Hausig, F. H. Sobotta, F. Richter, D. O. Harz, A. Traeger and J. C. Brendel, *ACS Appl. Mater. Interfaces*, 2021, **13**, 35233–35247.
52 L. Du, C. Wang, L. Meng, Q. Cheng, J. Zhou, X. Wang, D. Zhao, J. Zhang, L. Deng, Z. Liang, A. Dong and H. Cao, *Biomaterials*, 2018, **176**, 84–93.
53 L. Parhamifar, A. K. Larsen, A. C. Hunter, T. L. Andresen and S. M. Moghimi, *Soft Matter*, 2010, **6**, 4001–4009.
54 D. Gugutkov, C. González-García, J. C. R. Hernández, G. Altankov and M. Salmerón-Sánchez, *Langmuir*, 2009, **25**, 10893–10900.
55 J. E. Schwarzbauer, *J. Cell Biol.*, 1991, **113**, 1463–1473.
56 J. F. Dubern, A. L. Hook, A. M. Carabelli, C. Y. Chang, C. A. Lewis-Lloyd, J. C. Luckett, L. Burroughs, A. A. Dundas, D. J. Humes, D. J. Irvine, M. R. Alexander and P. Williams, *Sci. Adv.*, 2023, **9**(4), DOI: 10.1126/sciadv.add7474.

